Amorphous silicon waveguides for microphotonics

M. J. A. de Dood[a] and A. Polman
FOM Institute for Atomic and Molecular Physics, Kruislaan 407, 1098 SJ Amsterdam, The Netherlands

T. Zijlstra and E. W. J. M. van der Drift
Delft Institute of Microelectronics and Submicron Technology, P.O. Box 5053, 2600 GB Delft, The Netherlands

(Received 11 March 2001; accepted for publication 18 April 2002)

Amorphous silicon *a*-Si was made by ion irradiation of crystalline silicon with 1×10^{15} Xe ions cm^{-2} at 77 K in the 1–4 MeV energy range. Thermal relaxation of the amorphous network at 500 °C for 1 h leads to an amorphous layer with a refractive index of $n=3.73$, significantly higher than that of crystalline silicon ($n=3.45$ at $\lambda=1.55$ μm). *a*-Si can thus serve as a waveguide core in Si based optical waveguides. Channel waveguides were made by anisotropic etching of a 1.5 μm silicon-on-insulator structure that was partly amorphized. Transmission measurements of these waveguides as function of the amorphous silicon length show that the *a*-Si part of the waveguides exhibit a modal propagation loss of 70 cm^{-1} (0.03 dB μm^{-1}) and a bulk propagation loss of 115 cm^{-1} (0.05 dB μm^{-1}). Losses due to sidewall roughness are estimated, and are negligible compared to the modal loss. © *2002 American Institute of Physics.* [DOI: 10.1063/1.1486055]

I. INTRODUCTION

Silicon is the most widely used semiconductor material in current electronic devices, because of its excellent electronic properties. Single crystalline Si of high quality is available and the processing and microfabrication of Si are well known. Since silicon is transparent in the near infrared, Si is also an ideal optical material. Si-based waveguides may serve as optical interconnects on Si integrated circuits, or to distribute optical clock signals on a microprocessor. In such cases, using Si provides the advantage of integration with existing electronic circuits. So far, optical waveguide technology in silicon is not well developed. Fabrication of waveguides in Si requires a core with a higher refractive index than that of crystalline Si (*c*-Si).

Amorphous Si (*a*-Si) is an interesting candidate as a core material. While the density of pure *a*-Si is 1.8% lower than that of *c*-Si,[1] the refractive index of pure *a*-Si, at near-infrared wavelengths, is higher than that of *c*-Si.[2–5] Amorphous silicon can thus be used as a waveguide core material on crystalline Si. As pure *a*-Si contains a large density of point defects and dangling bonds, the optical absorption at near-infrared wavelengths can be substantial. These point defects can be passivated to some extent by incorporation of hydrogen. In fact, hydrogenated *a*-Si made by deposition shows excellent electrical quality, and relatively low optical absorption.[6]

Amorphous silicon has already received a lot of interest both from a fundamental point of view and because of its possible use in solar cells and optoelectronic devices. Hydrogenated *a*-Si films can be deposited using a number of different techniques, including plasma enhanced chemical vapor deposition (CVD), rf sputtering, and hot-filament CVD. The hydrogen content, void density, structural properties as well as optical and electronic properties have been studied intensively and depend critically on the exact processing conditions. In contrast, *a*-Si made by ion irradiation of crystalline silicon has reproducible properties that are insensitive to the preparation details, while voids seem to be absent in this material.[7] Heat treatment of pure *a*-Si made by ion irradiation induces structural relaxation[8] and reduces the defect density, which leads to an improvement in the optical and electronic properties. Overall, it seems that hydrogenated *a*-Si has better transparency in the near-infrared than pure *a*-Si. However, pure *a*-Si can be made more easily in a Si processing sequence, as it requires a single ion implantation step. Furthermore, pure *a*-Si has larger thermal stability then hydrogenated *a*-Si. Given these pros and cons of pure *a*-Si, it seems interesting to study its applicability in microphotonic integrated circuits. In this article we study the properties of amorphous silicon waveguides made using silicon-on-insulator (SOI) substrates and discuss the feasibility of *a*-Si waveguides for silicon microphotonic channel waveguides and optical interconnects, and as a guiding layer in two-dimensional photonic crystals.

II. PROPERTIES OF AMORPHOUS SILICON

To study the amorphization and structural relaxation of *a*-Si, crystalline Si(100) samples were mounted on a copper block that was kept at liquid nitrogen temperature. Samples were irradiated with 1×10^{15} Xe ions cm^{-2} in the 1–4 MeV energy range to form amorphous layers of different thickness. All irradiations were done with the ion beam incident under an angle of 7° with the surface normal to avoid ion channeling effects along the (100) crystal direction. After irradiation the amorphous silicon was heat treated at 500 °C for 1 h in a vacuum tube furnace (base pressure $<10^{-6}$ mbar). The amorphous layer thickness was measured by Rutherford backscattering spectrometry (RBS) channeling measurements using 2 MeV He^{+} ions at a scattering angle of

[a]Author to whom correspondence should be addressed; electronic mail: m.d.dood@amolf.nl

 © 2002 American Institute of Physics

Downloaded 05 Jun 2013 to 132.229.96.114. This article is copyrighted as indicated in the abstract. Reuse of AIP content is subject to the terms at: http://jap.aip.org/about/rights_and_permissions

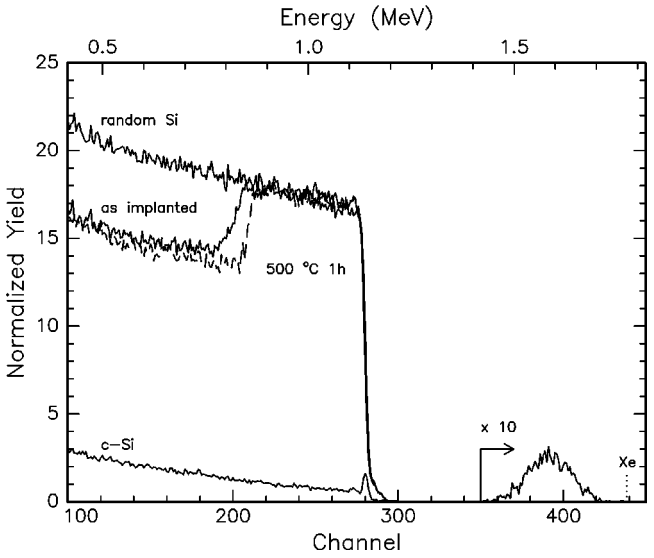

FIG. 1. RBS channeling spectra of amorphous silicon made by ion irradiation of crystalline Si with 1.0×10^{15} Xe ions cm^{-2}. The Xe ion energy was 1 MeV. Spectra are shown for the as implanted sample and for a sample annealed for 1 h at 500 °C. For comparison a channeling spectrum of crystalline Si and a random Si spectrum are shown as well. The surface channel of Xe is indicated in the figure and the Gaussian distribution of Xe ions is clearly visible.

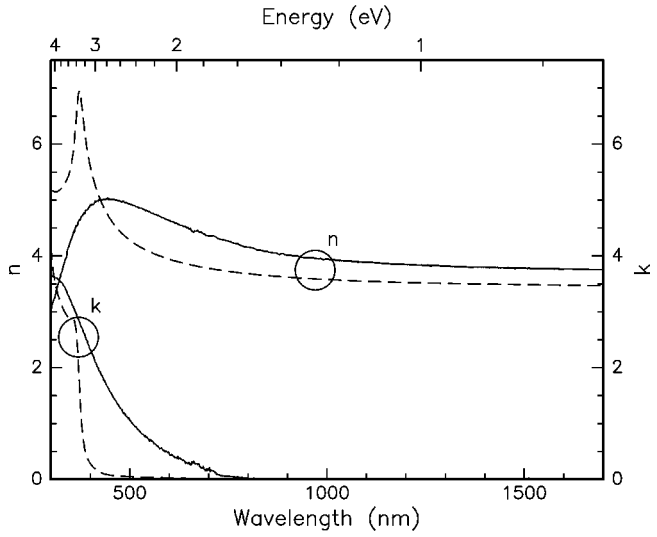

FIG. 2. Real (n) and imaginary (k) part of the index of refraction for relaxed amorphous silicon (drawn line) as function of wavelength, obtained from spectroscopic ellipsometry measurements. The index is compared to literature values for crystalline silicon (dashed lines) (see Ref. 22). In the near-infrared part of the spectrum ($\lambda>1100$ nm) the refractive index of amorphous is typically 0.3 higher than that of crystalline silicon, while the absorption is small.

165°. Variable angle spectroscopic ellipsometry in the 300–1700 nm wavelength was used to determine the refractive index of a-Si and to obtain independent information on the amorphous layer thickness.

The RBS channeling measurements for 1 MeV Xe irradiation are shown in Fig. 1. The data for ion irradiated samples are compared to channeling and random spectra of unirradiated crystalline Si. As can be seen, the Si signal follows the random height starting from the Si surface channel around channel 280, up to a certain depth in the sample for both the as-implanted and the sample annealed at 500 °C for 1 h. Annealing leads to the removal of point defects and amorphous pockets in the c-Si near the a-Si/c-Si interface, which sharpens the interface. In addition, solid phase epitaxial crystallization takes place at a growth rate of 0.083 Å/s at 500 °C[9,10] leading to a shift of the interface. This explains the difference in channeling spectra between the as-implanted and annealed samples. The Gaussian shaped profile around channel 390 is due to the implanted Xe ions. The peak of the implanted Xe distribution is roughly at the center of the a-Si thickness, and the Xe peak concentration is ~0.08 at. %. From similar channeling measurements and annealing studies we conclude that all samples irradiated with 1×10^{15} Xe ions cm^{-2} in the energy range 1–4 MeV, became amorphous up to the surface. The amorphous silicon thickness after annealing ranged from 0.6 μm for 1 MeV irradiation to 2.0 μm for 4 MeV irradiation.

Figure 2 shows the measured complex refractive index of amorphous silicon, made by 1 MeV Xe irradiation, after thermal relaxation (drawn line) compared to literature values for crystalline silicon (dashed line). After relaxation the ellipsometry data for wavelengths longer than 1.2 μm can be described with a lossless layer with a refractive index ~0.3 higher than that of crystalline silicon. To obtain the layer thickness accurately the ellipsometry data was first fitted to a model assuming a transparent layer in the range $\lambda>1200$ nm.[11] The refractive index was then obtained for the entire wavelength range by point by point fitting of the complex refractive index, while keeping the layer thickness fixed. By comparing data for samples made using different Xe ion energies it was found that the optical properties are independent of layer thickness. Also, samples annealed for 2 h at 500 °C or for 1 h at 550 °C gave the same results. The density of pure amorphous silicon is lower than that of crystalline silicon[1] and thus a density difference cannot explain the higher refractive index. Hence the high refractive index at infrared wavelengths must be attributed to a difference in the electronic bandstructure. Such a difference is apparent from the data near the direct band-to-band transitions in the visible part of the spectrum as observed in Fig . 2. Ellipsometry as performed here is not sensitive to very small optical absorption. Given the experimental error on the ellipsometry data, an upper limit of the loss coefficient of amorphous silicon at 1.5 μm is found: 100 cm^{-1}.

III. AMORPHOUS SILICON WAVEGUIDES

To further investigate the optical losses of a-Si, commercially available silicon-on-insulator (SOI) substrates with a 1.5 μm thick (100) oriented p-type (14–22 Ω cm) Si layer on a 3.0 μm thick SiO_2 layer grown by wet thermal oxidation were ion irradiated with 1×10^{15} 2 MeV Xe ions cm^{-2} at $T=77$ K. The irradiation, followed by thermal relaxation at 500 °C for 2 h leads to the formation of a ~1.2 μm thick amorphous silicon layer. During irradiation part of the SOI substrate was masked leading to a triangularly shaped amorphous silicon surface layer on the substrate (see inset in Fig. 4).

Downloaded 05 Jun 2013 to 132.229.96.114. This article is copyrighted as indicated in the abstract. Reuse of AIP content is subject to the terms at: http://jap.aip.org/about/rights_and_permissions

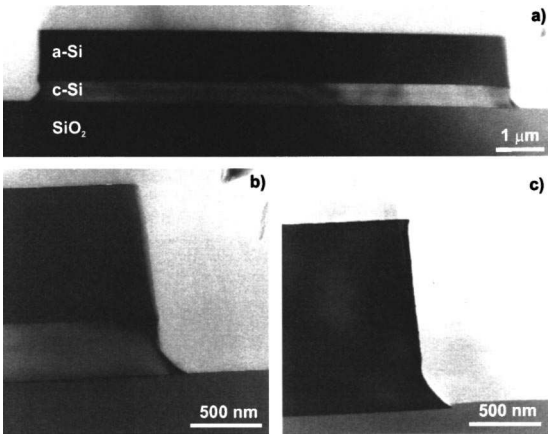

FIG. 3. Cross section TEM images of amorphous silicon channel waveguides on *c*-Si on SiO_2; (a) cross section of the amorphized crystalline region; (b) sidewall of *a*-Si guide; and (c) sidewall of *c*-Si guide. The thickness of the cross sections is 610 nm (b) and 310 nm (c).

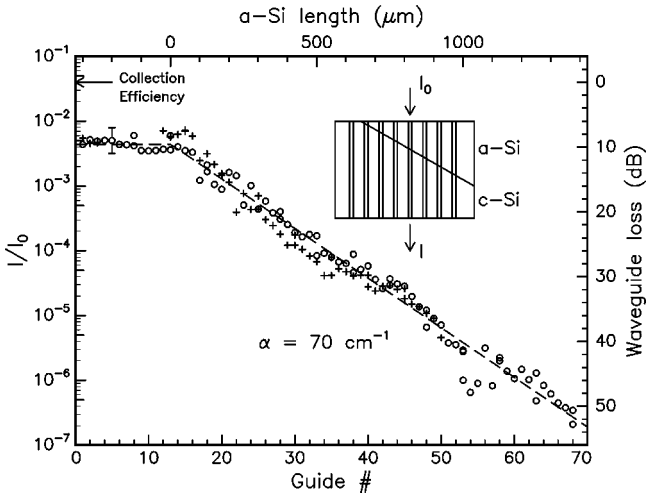

FIG. 4. Measured transmission (I/I_0) of *c*-Si waveguides with a short *a*-Si section as function of guide number (bottom axis) and *a*-Si length (top axis). The collection efficiency is estimated and is indicated on the left axis and is used as the 0 dB point of the waveguide loss indicated on the right axis. Measurements are shown after structural relaxation at 500 °C for 2 h (○) and after additional annealing at 500 °C for 1 h in a forming gas (10% H_2/90% N_2) atmosphere (+). A schematic representation of the sample geometry is shown in the inset.

After irradiation, a series of 10 μm wide waveguides at a 50 μm repeat distance were defined using electron-beam lithography and deep anisotropic etching. Mask patterns were defined in a resist double layer consisting of a 400 nm thick hard baked photoresist layer (HPR 504), with an 80 nm thick silicon containing negative tone *e*-beam resist (SNR) on top. After *e*-beam exposure (100 kV, 150 $\mu C\,cm^{-2}$) the pattern was developed for 20 s in xylene and rinsed for 30 s in iso-propyl-alcohol. The pattern was then anisotropically transferred in the bottom photoresist layer by low pressure O_2 reactive ion etching at room temperature ($p=0.3$ Pa, 0.07 W cm^{-2} rf power density, −180 V dc bias). Before etching the underlying Si, a dip in hydrofluoric acid (4%) was used to remove the thin native oxide. The pattern was then transferred in the silicon by electron-cyclotron resonance (ECR) driven plasma etching using a low pressure (0.1 Pa) SF_6/O_2 gas mixture (5.6:1.0) at −95 °C. A microwave power of 400 W was used, combined with a −15 V dc bias, resulting in an etch rate of ~300 nm min^{-1} and anisotropic etch profiles.[12] All patterning processes were controlled *in situ* by laser interferometry. The Si was etched back till the etching stopped at the underlying oxide layer, resulting in 1.5 μm high Si profiles.[13]

Figure 3 shows bright field cross sectional transmission electron microscopy (TEM) images of the waveguides taken using 300 kV electrons. Cross sections were first sawcut to 0.5–1 mm thickness, then thinned to 15 μm thickness by mechanical grinding and polishing, and finally ion milled with 5 kV Ar ions to electron transparency. Figure 3(a) shows the waveguide structure of the amorphous Si waveguide. The cross section shows a 1.06 μm thick amorphous Si region on top of a 0.45 μm crystalline Si layer on a 3.0 μm thick SiO_2 layer. As can be seen, the anisotropic ECR etching process has proceeded continuously through the *a*-Si/*c*-Si interface and leads to a similar sidewall angle for both materials. Figures 3(b) and 3(c) zoom in on the sidewalls of the *a*-Si waveguide and *a*-Si waveguide, respectively. They show small sidewall roughness, as will be discussed further on.

IV. RESULTS AND DISCUSSION

For optical transmission measurements, waveguide samples were sawcut to ≈7 mm length. The end faces were mechanically polished in order to attain an optimal light coupling into the waveguides. Transmission measurements at $\lambda = 1.49$ μm were performed by coupling an InGaAsP laser diode into the waveguides using a tapered optical fiber. 6% of the input power was split off to monitor the input power from the laser. The fiber alignment was controlled using piezoelectric actuators. Mode images were obtained by imaging the light from the output facet on an infrared camera using a 10× microscope objective. For transmission measurements, the output mode was collected by a Ge diode detector and was compared to the input power monitored simultaneously on an identical Ge diode detector.

Figure 4 shows the measured transmission (open circles) for a series of 70 waveguides. A schematic of the measurement setup with the amorphous and crystalline parts of the waveguides indicated is shown in the inset. The first ~12 waveguides are crystalline along their full length. By moving the input fiber along the horizontal direction on the sample, waveguides with an amorphous section of increasing length are probed. As can be seen, the measured transmission drops exponentially with increasing *a*-Si length. From the angle of the triangular amorphous region it is known that the amorphous silicon length increases by 25 μm per guide. This information was used to convert the horizontal scale to a length scale (top axis). The best fit to the data (dashed line in Fig. 4) results in an extinction coefficient of $\alpha = 70\,cm^{-1}$ (0.03 dB μm^{-1}). This is consistent with the upper limit of 100 cm^{-1} derived from ellipsometry in Sec. II.

The transmission in Fig. 4 is measured relative to the input power in the tapered fiber and thus contains both the coupling loss and collection efficiency in our setup. The col-

Downloaded 05 Jun 2013 to 132.229.96.114. This article is copyrighted as indicated in the abstract. Reuse of AIP content is subject to the terms at: http://jap.aip.org/about/rights_and_permissions

lection efficiency was measured to be 4% by directly collecting the laser light from the tip of the tapered fiber without a waveguide. This value is indicated by the arrow in Fig. 4. The right axis in Fig. 4 shows waveguide loss in dB, corrected for this collection efficiency. The combined transmission and coupling losses through the 7 mm long crystalline waveguides (i.e., without *a*-Si) is less than 9 dB, which corresponds to $\alpha < 3\ \mathrm{cm}^{-1}$. This is insignificant compared to the value of 70 cm^{-1} measured for the *a*-Si waveguides.

In the remainder of this article we will discuss the nature of the optical loss of *a*-Si waveguides. Several loss mechanisms should be considered, including coupling losses, scattering losses due to sidewall roughness, and intrinsic material losses. Free carrier absorption can in our case be neglected since the experiments were carried out on lightly doped Si.[14]

Coupling loss occurs when coupling from the tapered input fiber to the waveguide and also when the mode crosses the junction between the *c*-Si and *a*-Si section of the waveguides as they have different optical mode sizes. Both types of coupling loss can be estimated from the mode overlap that can be calculated based on measured mode profiles. The measured output modes of the waveguides and the tapered fiber are both described satisfactorily by Gaussian shaped mode profiles. Assuming optimum alignment from fiber to waveguide, a lower limit of the coupling loss of 0.45 dB can be estimated. The loss occurring at the transition from the *c*-Si to *a*-Si part of the waveguide is calculated using the waveguide modes obtained from a finite element simulation. The loss due to mode mismatch is estimated to be 0.25 dB (94% transmission). Note that the coupling losses lead to a vertical shift of the data in Fig. 4 and do not affect the exponential decay observed.

To investigate scattering losses due to sidewall roughness, TEM images of the waveguide cross section [see Figs. 3(b) and 3(c)] and scanning electron microscopy (SEM) images (not shown) taken from the top and along the propagation direction were used to measure roughness of both the *c*-Si and *a*-Si waveguide sidewalls. A sidewall roughness (σ) of $\sim$5 nm for *c*-Si and $\sim$10 nm for *a*-Si is derived. Within the experimental resolution of the SEM ($\sim$5 nm), these values are confirmed by the SEM images taken from the top. As can be seen in Fig. 3(b) the roughness at the *a*-Si–*c*-Si interface is small, and is expected to be of an atomic scale.[15] To calculate the scattering losses due to surface roughness, we use an expression derived by Tien[16] based on the Rayleigh criterion:

$$\alpha_s = \left(\frac{4\pi}{\lambda_2}\right)^2 \left(\frac{1}{2}\frac{\sin^3\theta}{\cos\theta}\right)\left(\frac{1}{t_g + (1/p) + (1/q)}\right)\sigma^2, \qquad (1)$$

where σ^2 is the variance of the surface roughness, λ_2 is the wavelength in the guiding layer, t_g is the thickness of the guiding layer. θ is the mode angle of the mode propagating in the waveguide, and $1/p$ and $1/q$ are the penetration depths of the mode into the cladding. Using the calculated propagation constant of the waveguides as obtained from a finite element simulation and the measured values for σ, the scattering loss can be estimated to be 0.1 cm^{-1} (0.4 $\mathrm{dB\,cm}^{-1}$) for the *c*-Si guide and 0.4 cm^{-1} (1.6 $\mathrm{dB\,cm}^{-1}$) for the *a*-Si waveguide. These values are much lower than the loss of 70 cm^{-1} found from Fig. 4. In fact, a sidewall roughness of $\sigma = \sim 200$ nm is needed to obtain a loss figure of 70 cm^{-1}, which would strongly disagree with the TEM data of Fig. 3. Therefore we conclude that the measured loss of the *a*-Si waveguide is mainly due to intrinsic absorption in the amorphous silicon itself. To convert the modal loss of 70 cm^{-1} to the intrinsic absorption coefficient of amorphous silicon, the confinement factor of the waveguide mode should be taken into account. Both from the experimentally measured mode and the finite element calculation a typical confinement factor of 60% is estimated. The absorption coefficient of amorphous silicon at 1.5 μm is thus estimated to be 115 cm^{-1} (0.05 $\mathrm{dB}\,\mu\mathrm{m}^{-1}$).

It is known that hydrogen can passivate point defects in *a*-Si and could thus reduce the absorption observed at 1.5 μm. To study this, the waveguide sample as described above was annealed in a forming gas atmosphere (10% H_2/90% N_2) at 500 °C for 1 h. Given a typical diffusion constant of H_2 in silicon, hydrogen could diffuse $\sim$30 μm into the *a*-Si network and passivate defects inside the *a*-Si. Other experiments indicate that under these conditions concentrations of a few at. %[17] atomic hydrogen can be incorporated in *a*-Si. The + symbols in Fig. 4 show the transmission measured after this hydrogen treatment. It cannot be distinguished from the transmission measured before annealing in hydrogen. Apparently it is not possible to passivate defects responsible for absorption losses in *a*-Si made by MeV ion-irradiation by the thermal treatment described above.

The optical losses in *a*-Si waveguides described in this article (0.05 $\mathrm{dB}\,\mu\mathrm{m}^{-1}$) make *a*-Si an ideal waveguide core material in Si microphotonic circuits. With typical dimensions well below 100 μm, intrinsic losses on the scale of such devices would be quite tolerable. As the fabrication of *a*-Si using ion irradiation is fully compatible with Si microfabrication and integrated circuit processing this enables the fabrication of waveguides in Si, with the vertical confinement provided by the higher index *a*-Si. To keep the dimensions of these devices as small as possible and to obtain a high packing density requires waveguides that can make very small bends. With the high refractive index of *a*-Si a bending radius of order 1 μm may be achieved.[18,19] Alternatively, two-dimensional (2D) photonic crystal structures have been proposed to achieve high transmission for 90° bends with very small radius of curvature.[20,21] In the remainder of this article we will describe how a combination of *a*-Si waveguides and Si photonic crystal technology may be used to achieve such small bending radius for the important telecommunication wavelength of 1.5 μm.

Figure 5 shows a SEM image of 2D Si photonic crystal waveguide bend designed for operation at 1.5μm wavelength. The device consists of an array of 205 nm diameter cylindrical Si rods placed on a square lattice with a lattice constant $a = 570$ nm. The rods are 5 μm long and have a 2 μm thick *a*-Si top section to confine the light in the vertical direction. Input and output channel waveguides to test the device are defined as well. The inset zooms in on the entrance of the photonic crystal waveguide and clearly shows the removed row of rods and the input waveguide. The mask

Downloaded 05 Jun 2013 to 132.229.96.114. This article is copyrighted as indicated in the abstract. Reuse of AIP content is subject to the terms at: http://jap.aip.org/about/rights_and_permissions

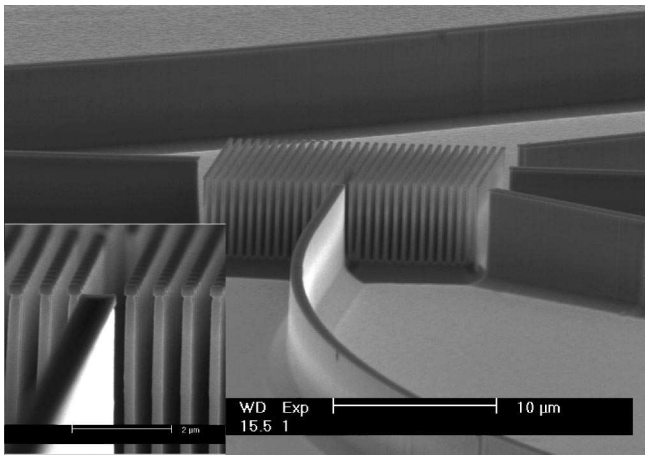

FIG. 5. Example of a Si photonic crystal device with a 2 μm thick a-Si top section to confine the light vertically. The device consists of an array of 205 nm diameter cylindrical Si rods placed on a square lattice with a lattice constant $a=570$ nm. The rods are 5 μm long and have a 2 μm thick a-Si top section to confine the light vertically. The remaining photoresist is clearly visible on top of the pillars. A row of rods is removed from the array to define a 90° waveguide bend. Input and output channel waveguides to test the device are defined as well. The inset zooms in on the entrance of the photonic crystal waveguide and clearly shows the removed row of rods together with the input waveguide.

pattern for this device was defined by *e*-beam lithography and oxygen reactive ion etching following the same processing as for the channel waveguides discussed earlier and described in detail in Ref. 12. The Si etch process was more carefully tuned because of the smaller feature sizes and higher aspect ratios involved. The photonic waveguide bend structures are dry etched in an ECR plasma of SF_6/O_2 (7.3:1) at a pressure of 0.1 Pa, a substrate temperature of -97 °C, a μwave power of 400 W and a dc bias of -12 V, resulting in an etch rate of about 150 nm min^{-1}. Details of the device fabrication procedure are published elsewhere.[12]

The next challenge is to characterize the transmission characteristics of the bends. In this analysis, the main problem is the fact that the mm-long a-Si input and output waveguides suffer from high loss. This once again shows that in studies of microphotonic materials, the coupling to the outside macroscopic world is a matter of great importance and concern. In future microphotonic integrated devices, such problems can be minimized by integrating as many optical functions as possible on a single optical chip.

V. CONCLUSIONS

We have fabricated amorphous silicon (a-Si) waveguides by combining MeV Xe ion irradiation with anisotropic etching techniques. Transmission measurements on 10 μm wide waveguides with different a-Si length revealed a modal absorption coefficient of 70 cm^{-1} (0.03 dB μm^{-1}) at a wavelength of 1.5 μm. Annealing of the waveguides in a hydrogen atmosphere did not improve the optical properties of the waveguides. The scattering loss of the waveguides due to sidewall roughness was calculated and found to be insignificant compared to the total modal loss. Taking the confinement factor of 60% into account the intrinsic absorption coefficient of a-Si made by ion irradiation is found to be 115 cm^{-1} (0.05 dB μm^{-1}). Since the processing of a-Si made by ion irradiation is compatible with standard Si microfabrication and integrated circuit technology, a-Si can be used to vertically confine light in microphotonic devices with dimensions well below 100 μm. As an example, a 2D photonic crystal device is presented in which the vertical confinement may be achieved by index guiding in a 2 μm thick a-Si top section.

ACKNOWLEDGMENTS

Rene Koper of the Surface Preparation Laboratory is gratefully acknowledged for mechanical polishing of the waveguide endfaces. F.D. Tichelaar and T.R. de Kruijff at the National Center for HREM at the Delft University of Technology are acknowledged for the TEM sample preparation and analysis. This work is part of the research program of the Foundation for Fundamental Research on Matter (FOM) and was made possible by financial support from the Dutch Foundation of Scientific Research (NWO).

[1] J. S. Custer, M. O. Thompson, D. C. Jacobson, J. M. Poate, S. Roorda, and W. C. Sinke, Appl. Phys. Lett. **64**, 437 (1994).
[2] G. K. Hubler, C. N. Waddell, W. G. Spitzer, J. E. Fredrickson, S. Prussin, and R. G. Wilson, J. Appl. Phys. **50**, 3294 (1979).
[3] C. N. Waddell, W. G. Spitzer, J. E. Fredrickson, G. K. Hubler, and T. A. Kennedy, J. Appl. Phys. **55**, 4361 (1984).
[4] M. Fried, T. Lohner, W. A. M. Aarnink, L. J. Hanekamp, and A. van Silfhout, J. Appl. Phys. **71**, 5260 (1992).
[5] R. Reitano, M. G. Grimaldi, P. Baeri, A. Borghesi, and A. Sassella, Thin Solid Films **233**, 203 (1993).
[6] G. Cocorullo, F. G. D. Corte, I. Rendina, C. Minarini, A. Rubino, and E. Terzini, Opt. Lett. **21**, 2002 (1996).
[7] D. L. Williamson, S. Roorda, M. Chicoine, R. Tabti, P. A. Stolk, S. Acco, and F. W. Saris, Appl. Phys. Lett. **67**, 226 (1995).
[8] K. Laaziri, S. Kycia, S. Roorda, M. Chicoine, J. L. Robertson, J. Wang, and S. C. Moss, Phys. Rev. B **60**, 13520 (1999).
[9] J. S. Custer, M. O. Thompson, and P. H. Bucksbaum, Appl. Phys. Lett. **53**, 1402 (1988).
[10] G. L. Olson and J. A. Roth, Mater. Sci. Rep. **3**, 1 (1988).
[11] To fit the ellipsometry data correctly, a 2.41 nm thick native oxide layer on top of the amorphous silicon was used in the model.
[12] T. Zijlstra, E. van der Drift, M. J. A. de Dood, E. Snoeks, and A. Polman, J. Vac. Sci. Technol. B **17**, 2734 (1999).
[13] The a-Si layer has a 30% lower etch rate than the (100)-oriented c-Si. The etching process was controlled on the a-Si part of the sample, thus slightly overetching the c-Si part.
[14] The free carrier concentration in the p-type Si waveguides (14–22 Ω cm) is $\sim 1.0\times 10^{15}$ cm^{-3}. Using an absorption cross section of 0.64×10^{-17} cm^2, this leads to a loss coefficient $\alpha\sim 6\times 10^{-3}$, so that free carrier absorption can be safely neglected; M. A. Green, *Silicon Solar Cells* (University of New South Wales, Sydney, 1995).
[15] M. Lohmeier, S. de Vries, J. S. Custer, E. Vlieg, M. S. Finney, F. Priolo, and A. Battaglia, Appl. Phys. Lett. **64**, 1803 (1994).
[16] P. K. Tien, Appl. Opt. **10**, 2395 (1971).
[17] S. Acco, D. L. Williamson, P. A. Stolk, F. W. Saris, M. J. van den Boogaard, W. C. Sinke, W. F. van der Weg, S. Roorda, and P. C. Zalm, Phys. Rev. B **53**, 4415 (1996).
[18] E. A. J. Marcatili, Bell Syst. Tech. J. **7**, 2103 (1969).
[19] R. L. Espinola, F. P. R. U. Ahmad, M. J. Steel, and R. M. Osgood Jr., Opt. Express **8**, 517 (2001).
[20] A. Mekis, J. C. Chen, I. Kurland, S. Fan, P. R. Villeneuve, and J. D. Joannopoulos, Phys. Rev. Lett. **77**, 3787 (1996).
[21] S.-Y. Lin, E. Chow, V. Hietala, P. R. Villeneuve, and J. D. Joannopoulos, Science **282**, 274 (1998).
[22] E. D. Palik, *Handbook of Optical Constants of Solids* (Academic, Boston, 1991), Vol. 1.

Downloaded 05 Jun 2013 to 132.229.96.114. This article is copyrighted as indicated in the abstract. Reuse of AIP content is subject to the terms at: http://jap.aip.org/about/rights_and_permissions